The EMBO Journal (2008) 27, 3221–3234 | © 2008 European Molecular Biology Organization | Some Rights Reserved 0261-4189/08
www.embojournal.org

THE EMBO JOURNAL

EMBO open

VAC14 nucleates a protein complex essential for the acute interconversion of PI3P and PI(3,5)P_2 in yeast and mouse

Natsuko Jin[1,7], Clement Y Chow[2,7], Li Liu[3], Sergey N Zolov[1], Roderick Bronson[4], Muriel Davisson[5], Jason L Petersen[1], Yanling Zhang[1], Sujin Park[1], Jason E Duex[1], Daniel Goldowitz[6], Miriam H Meisler[2,*] and Lois S Weisman[1,*]

[1]Department of Cell and Developmental Biology and Life Sciences Institute, University of Michigan, Ann Arbor, MI, USA, [2]Department of Human Genetics, University of Michigan, Ann Arbor, MI, USA, [3]Department of Anatomy and Neurobiology, University of Tennessee Health Science Center, Memphis, TN, USA, [4]Department of Pathology, Harvard Medical School, Boston, MA, USA, [5]Mutant Resources Program, The Jackson Laboratory, Bar Harbor, ME, USA and [6]Department of Medical Genetics, University of British Columbia, Vancouver, BC, USA

The signalling lipid PI(3,5)P_2 is generated on endosomes and regulates retrograde traffic to the trans-Golgi network. Physiological signals regulate rapid, transient changes in PI(3,5)P_2 levels. Mutations that lower PI(3,5)P_2 cause neurodegeneration in human patients and mice. The function of Vac14 in the regulation of PI(3,5)P_2 was uncharacterized previously. Here, we predict that yeast and mammalian Vac14 are composed entirely of HEAT repeats and demonstrate that Vac14 exerts an effect as a scaffold for the PI(3,5)P_2 regulatory complex by direct contact with the known regulators of PI(3,5)P_2: Fig4, Fab1, Vac7 and Atg18. We also report that the mouse mutant *ingls* (infantile gliosis) results from a missense mutation in Vac14 that prevents the association of Vac14 with Fab1, generating a partial complex. Analysis of *ingls* and two additional mutants provides insight into the organization of the PI(3,5)P_2 regulatory complex and indicates that Vac14 mediates three distinct mechanisms for the rapid interconversion of PI3P and PI(3,5)P_2. Moreover, these studies show that the association of Fab1 with the complex is essential for viability in the mouse.

The EMBO Journal (2008) **27,** 3221–3234. doi:10.1038/emboj.2008.248; Published online 27 November 2008
Subject Categories: membranes & transport; neuroscience
Keywords: *pale tremor*; phosphatidylinositol 3,5-bisphosphate; PIKfyve; *Saccharomyces cerevisiae*

*Corresponding author. LS Weisman or MH Meisler, Life Sciences Institute, 210 Washtenaw Avenue, Room 6437, The University of Michigan, Ann Arbor, MI 48109-2216, USA.
Tel.: +734 647 2539; Fax: +734 615 5499;
E-mail: lweisman@umich.edu; meislerm@umich.edu
[7]These authors contributed equally to this work

Received: 28 August 2008; accepted: 23 October 2008; published online: 27 November 2008

Introduction

Phosphoinositide phosphate (PIP) lipids are transiently generated on the cytoplasmic face of selected intracellular membranes. Spatial localization of the lipid kinases and phosphatases that generate specific PIPs produces unique PIP tags on different membrane compartments (Matteis and Godi, 2004; Behnia and Munro, 2005; Bolis *et al*, 2007). PIPs function through recruitment of specific effector proteins, which in turn regulate ion channels, membrane fission and fusion, and formation of membrane tubules. PI(3,5)P_2 is synthesized by phosphorylation of PI3P. Both PI3P and PI(3,5)P_2 are generated in the endomembrane system, a heterogeneous system of membranes involved in traffic to and from the plasma membrane, the lysosome, and the Golgi (Di Paolo and De Camilli, 2006). PI(3,5)P_2 is a minor PIP present at <0.1 and $<0.05\%$ of total PI lipids in yeast and mammalian cells, respectively, compared with the more typical values of 2.5 and 0.2% for PI3P (Bonangelino *et al*, 2002; Duex *et al*, 2006b; Zhang *et al*, 2007).

The dynamic interconversion of PI3P and PI(3,5)P_2 is regulated by at least five proteins in yeast: the lipid kinase Fab1p, lipid phosphatase Fig4p, the Fab1p activator Vac7p, the Fab1p inhibitor Atg18p, and Vac14p, a protein required for the activity of both Fab1p and Fig4p (Bonangelino *et al*, 1997, 2002; Gary *et al*, 1998, 2002; Dove *et al*, 2002, 2004; Rudge *et al*, 2004; Duex *et al*, 2006a, b; Efe *et al*, 2007). Homologues of Fab1p, Vac14p and Fig4p are found in all eukaryotes. In yeast, Vac14p, Fab1p and Fig4p are localized on the vacuole membrane (Bonangelino *et al*, 2002; Dove *et al*, 2004; Rudge *et al*, 2004; Duex *et al*, 2006a) and form a complex (Botelho *et al*, 2008). In mammalian cells, these proteins, also known as Fab1/PIKfyve/PIP5K3, Fig4/Sac3, and Vac14/ArPIKfyve, are located on early and late endosomes (Ikonomov *et al*, 2006; Rutherford *et al*, 2006). Association of the three mammalian proteins in cultured cells has been demonstrated by coimmunoprecipitation and cosedimentation (Sbrissa *et al*, 2007). Genetic analysis in yeast shows that Vac14p is required for Fab1p and Fig4p function (Bonangelino *et al*, 1997; Duex *et al*, 2006b), but the mechanism of this regulation is not known.

We recently described lethal null mutations of mammalian *Vac14* and *Fig4* that revealed the critical function of PI(3,5)P_2 for neuronal survival. A null mutation of *Fig4* in the *pale tremor* mouse results in the formation of vacuoles in the cell bodies of neurons of the central nervous system (CNS) and peripheral nervous system, with extensive degeneration of sensory neurons of the dorsal root ganglia (DRG) and juvenile lethality around the time of weaning (Chow *et al*, 2007). A null mutation of *Vac14* results in perinatal lethality with extensive degeneration of DRG neurons (Zhang *et al*, 2007). The level of PI(3,5)P_2 is reduced by approximately 50% in

cultured fibroblasts from both mutants. The increased sensitivity of neurons to mutations causing $PI(3,5)P_2$ deficiency could result from the high rate of membrane turnover required for maintenance of axonal and dendritic processes (Volpicelli-Daley and De Camilli, 2007). Vacuoles that contain the late endosome/lysosome marker LAMP-2 accumulate in cells deficient in *Fig4*, *Vac14* or *Fab1* (Ikonomov *et al*, 2006; Rutherford *et al*, 2006; Chow *et al*, 2007; Zhang *et al*, 2007), suggesting that failure to resolve late endosomal vesicles may be responsible for vacuole accumulation. Human patients who are compound heterozygotes for missense and null mutations of *Fig4* are affected by Charcot–Marie–Tooth type 4J, a severe peripheral neuronopathy (Chow *et al*, 2007; Zhang *et al*, 2008).

The *ingls* mouse, a spontaneous neurological mutant with autosomal recessive inheritance, arose at the Jackson Laboratory in 1991 (Bronson *et al*, 2003). We now report that a missense mutation of a conserved leucine residue in *Vac14* is the molecular defect in *ingls*. As the *ingls* mouse survives for up to 3 weeks after birth, postnatal phenotypes caused by defective Vac14 function could be characterized. Examination of the corresponding mutation in yeast *vac14*, combined with analysis of additional partially functional mutants of yeast *vac14* and *fab1*, led to the determination that Vac14 nucleates the $PI(3,5)P_2$ regulatory complex. The mutants led to the identification of specific regions of the Vac14 protein required for interaction with proteins in the complex. We also demonstrate that two additional regulators of the Fab1 kinase, Vac7p and Atg18p, reside within the complex. We find that formation of the complex is essential for the osmotic-stress-induced activation of Fab1. Analysis of the new *vac14* and *fab1* mutants provides insights into the organization of the $PI(3,5)P_2$ regulatory complex and its crucial function in the mammalian nervous system.

Results

Phenotype of the ingls mouse

The spontaneous mutation *ingls* (infantile gliosis) arose on the DBA/2J strain background and has been maintained by 23 generations of backcrossing to strain C57BL/6J to generate the congenic line B6. *ingls*. Homozygous *ingls* mutants exhibit reduced body size and diluted pigmentation that can be recognized as early as postnatal day 3 (P3) (Figure 1A). By P14, the mice exhibit a tremor and impaired motor function (Supplementary video). The frequency of affected offspring born from crosses between heterozygous carriers is consistent with Mendelian expectation (29/140, $P = 0.24$). However, the maximal survival for *ingls/ingls* homozygotes is 3 weeks, with continuous losses between P1 and P21. Histological analysis of the brain revealed greatly enlarged ventricles (Figure 1B, middle panel). Small areas with the appearance of spongiform degeneration are visible in several brain regions, including the thalamus, brain stem and cerebellar nucleus (Supplementary Figure S1A). This pattern resembles the more widespread degeneration in the *Fig4*-null mouse (Chow *et al*, 2007). However, spinal motor neurons and sensory neurons in the DRG remain intact during the lifetime of the *ingls* mutant (Supplementary Figure S1B). Intense staining for glial fibrillary acidic protein (GFAP) is evident throughout the *ingls* brain, suggesting widespread astrogliosis (Figure 1C and Supplementary Figure S2A). GFAP is sufficiently increased to be detected by western blot of cortical extracts (Supplementary Figure S2B). Increased GFAP staining is evident as early as E14.5 (not shown).

Genetic mapping of ingls

The *ingls* mutation was first mapped to an 18 Mb interval on distal mouse chromosome 8, between microsatellite markers *D8Mit86* and *D8Mit88*, by genotyping 31 affected F2 offspring from a cross between DBA/2J.*ingls*/+ and C57BL/6J (Bronson *et al*, 2003). Genotyping additional markers on chromosome 8 reduced the nonrecombinant region to a 5.7 Mb interval with the following gene order: SNP1 (111.6 Mb)—1/62—*ingls*—1/62—D8Mit88 (117.3 Mb) (Supplementary Figure S3A). This nonrecombinant region contains 63 annotated genes (Mouse Build 37.2, www.ensembl.org).

Identification of a mutation in Vac14

The *Vac14* gene spans the region between 113.1 and 113.2 Mb on chromosome 8, within the *ingls* nonrecombinant region. Based on similarities between the *ingls* phenotype and null mutations of *Vac14* and *Fig4* (Chow *et al*, 2007; Zhang *et al*, 2007), we tested *Vac14* as a candidate gene for *ingls*.

The 19 exons of *Vac14* were amplified from genomic DNA of an affected *ingls* homozygote and sequenced. Comparison with the wild-type sequence from strain C57BL/6J (Build 37.2, www.genome.ucsc.edu) identified the nucleotide substitution c.467T>G in exon 4 (Figure 1D). Strain DBA/2J, the strain of origin of the *ingls* mutation, contains the wildtype residue (not shown). The T>G substitution destroys a *Sac*I endonuclease site, which was used to genotype the $Vac14^{ingls}$ allele. The mutation results in substitution of an arginine residue for the evolutionarily invariant residue leucine 156 (Figure 1E). Western blot analysis of brain extracts revealed normal abundance of Vac14 protein in the mutant brain (Figure 1F).

Noncomplementation of ingls and a Vac14-null allele

To confirm the causal function of the Vac14-L156R mutation in the *ingls* phenotype, we assessed the ability of the $Vac14^{ingls}$ allele to complement the recessive lethality of the null allele $Vac14^{\beta-geo}$ ($Vac14^{-}$) (Zhang *et al*, 2007). Heterozygous *ingls* mice ($Vac14^{+/ingls}$) were crossed with null heterozygotes ($Vac14^{+/-}$). The $Vac14^{ingls/-}$ compound heterozygotes were born in the predicted Mendelian ratio of 25% but did not survive to weaning, showing that *ingls* is allelic with the null allele (Supplementary Figure S3B). The compound heterozygotes reproduced the phenotype of the *ingls* homozygote, with reduced body size and diluted pigmentation (Figure 1A), as well as enlarged ventricles (Figure 1B). The phenotypic similarity between $Vac14^{ingls/-}$ compound heterozygotes and *ingls* homozygotes, the failure of the *ingls* allele to rescue the null homozygote, and the mapping of *ingls* to an interval of chromosome 8 that includes *Vac14*, support the identification of Vac14-L156R as the *ingls* mutation. The survival of the compound heterozygotes to P14, compared with the neonatal lethality of null homozygotes, shows that the $Vac14^{L156R}$ allele retains partial function.

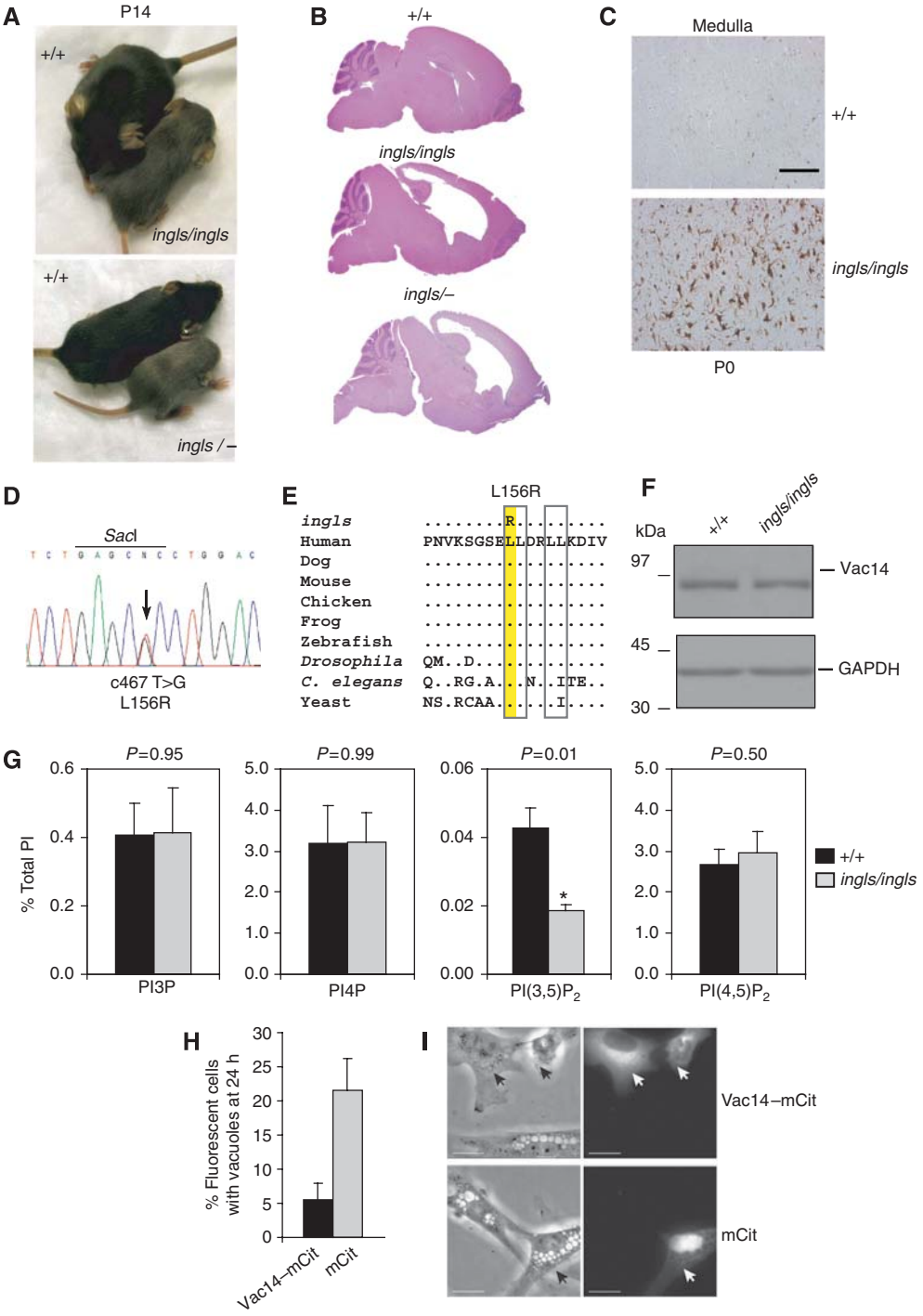

Figure 1 *ingls* is caused by the missense mutation *Vac14–L156R*. (**A**) *ingls* homozygous mice at postnatal day 14 (P14) display reduced body weight and diluted coat colour. *ingls/Vac14*$^{-}$ compound heterozygotes at P14 are similar in appearance. (**B**) Severe hydrocephalus and enlarged ventricles in *ingls* homozygote (P16) and *ingls/Vac14*$^{-}$ compound heterozygotes (P14) (H&E staining). (**C**) GFAP-stained astrocytes in neonatal *ingls*- and *Vac14*-null mice. (**D**) Sequence chromatogram from exon 4 of an *ingls/+* heterozygote demonstrates the c467 T>G nucleotide substitution. (**E**) The *ingls* mutation changes leucine 156 to arginine. Leucine 156 is evolutionarily invariant from yeast to mammals. Dots indicate amino-acid identity with human Vac14. (**F**) Western blot of Vac14 protein in brain extracts of wild-type and *ingls* mice. Loading control, GAPDH. (**G**) Reduced levels of PI(3,5)P_2 in cultured fibroblasts from *ingls* mice. (**H**, **I**) Rescue of vacuole formation by wild-type human *Vac14* cDNA. Primary fibroblasts from *ingls* mice transfected with the indicated plasmids. At 24 h, cells were fixed with 4% paraformaldehyde in PBS for 10 min, room temperature. (H). Fluorescent cells were scored for the presence of vacuoles. Mean ± s.d. for three independent experiments, >100 cells per experiment. (I) Representative cells are shown; arrows mark transfected cells. Bar, 20 μm.

Reduced levels of PI(3,5)P_2 and vacuolization of cultured ingls fibroblasts

Levels of phosphoinositide lipids were assessed in cultured *ingls* fibroblasts. In wild-type fibroblasts, PI(3,5)P_2 comprised 0.04% of total PI. In mutant *ingls* fibroblasts, PI(3,5)P_2 was reduced to 50% of normal, whereas the levels of PI3P, PI4P and PI(4,5)P_2 were unaffected (Figure 1G).

There is accumulation of intracellular cytoplasmic vacuoles in the cultured fibroblasts from *ingls* mice (Figure 1I, bottom). The vacuolated appearance of the *ingls* fibroblasts is similar to the fibroblasts from *Vac14*- and *Fig4*-null mice, indicating that the reduced level of $PI(3,5)P_2$ is responsible for the similarity (Chow *et al*, 2007; Zhang *et al*, 2007). Transfection of a construct expressing a wild-type human Vac14–mCit fusion protein reduced the frequency of vacuolized *ingls* fibroblasts from 20 to 5% (Figure 1H and 1I). Correction by wild-type Vac14 shows that the Vac14–L156R mutation is responsible for the *ingls* cellular phenotype. The stability of the mutant protein *in vivo* indicates that the Vac14–L156R protein is functionally impaired.

Prediction that Vac14 is composed entirely of HEAT repeats places the L156R mutation in repeat 4

HEAT repeats contain two anti-parallel helices connected by a short loop. These units often appear as a tandem series and provide surfaces for protein–protein interactions (Groves *et al*, 1999; Andrade *et al*, 2000). Previous analysis of the Vac14p sequence identified 1–3 HEAT repeats (Dove *et al*, 2002). As HEAT repeat sequences are degenerated, many bona fide repeats are not detected by motif detection programs.

Analysis of the Vac14 protein sequence with the repeat finding program REP set at a confidence threshold of $P_0 < 1e{-}6$ (http://www.embl-heidelberg.de/~andrade/papers/rep/search.html) (Andrade *et al*, 2000) predicted eight HEAT repeats in the *Saccharomyces cerevisiae* Vac14p sequence. One additional repeat was identified by REP in *Drosophila melanogaster* and *Schizosaccharomyces pombe* sequences and, by sequence similarity, was found in the *S. cerevisiae* sequence. A second analysis incorporated Vac14p sequences from 17 diverse species. Predicted HEAT repeats were defined by three criteria: (1) identification by REP in one or more species using no confidence threshold; (2) secondary structure prediction of two helices connected by a short loop; (3) alignment by visual inspection with HEAT repeat consensus sequences from the Pfam database. This analysis identified 21 potential HEAT repeats in *S. cerevisiae* Vac14p (Figure 2A). Many exhibit sequence similarity in all 17 species (not shown). Yeast Vac14p is thus most likely to contain a minimum of 9 HEAT repeats and as many as 21 repeats, which would comprise the entire protein. Analysis of human Vac14 predicted 17 repeats, 15 of which have homologues in *S. cerevisiae* Vac14p. The L156R mutation is located in helix B of HEAT repeat 4 (Figure 2A). A similar analysis accurately predicted the 50 HEAT repeats of TOR1 (Perry and Kleckner, 2003).

The L156R mutation disrupts Vac14 interaction with Fab1 but not Fig4

HEAT repeat proteins usually function as scaffolds with multiple binding partners (Groves *et al*, 1999; Andrade *et al*, 2000). The prediction that Vac14 may be composed entirely of HEAT repeats suggested that Vac14 may bind proteins that regulate $PI(3,5)P_2$ levels. Previous sedimentation and coimmunoprecipitation analysis demonstrated that mammalian Vac14, Fab1, and Fig4 associate with each other (Sbrissa *et al*, 2007). We tested potential interactions using the yeast two-hybrid test and found that human Vac14 interacts with Fab1 and Fig4 (Figure 2B). The *ingls* mutation, Vac14-L156R, specifically disrupts the interaction between Vac14 and Fab1 but retains interaction with Fig4 (Figure 2B). A third interaction of yeast Vac14p is self-association (Dove *et al*, 2002). We find that human Vac14 also interacts with itself and this interaction is unaffected by the Vac14–L156R mutation (Figure 2B). These data suggest that disruption of the interaction between Fab1 and Vac14 is the molecular basis for the *ingls* mutant phenotype.

Vac14p interacts with the known protein regulators of $PI(3,5)P_2$

To determine whether Vac14p interacts with the other proteins known to regulate $PI(3,5)P_2$ levels, we tested Vac7p and Atg18p, two additional regulators of yeast Fab1p. As Fab1p and Vac7p are large proteins, we performed a yeast two-hybrid test with constructs that expressed overlapping peptides from conserved regions of Fab1p and Vac7p. We found that Fab1p peptide 538–1085 and Vac7p peptide 394–918 interacted with yeast Vac14p in the yeast two-hybrid test (Figure 2C). Vac14p also interacts with full-length constructs of Fig4p and Atg18p and with itself (Figure 2C).

To determine whether each protein colocalizes with Vac14p *in vivo*, we generated a chromosomal integrant of a Vac14p fusion construct containing the fluorescent tag RFP–mCherry. Consistent with the yeast two-hybrid studies, Vac14p–mCherry colocalized on the vacuole membrane with GFP- or Venus-tagged Fab1p, Fig4p, Vac7p, and Atg18p (Supplementary Figure S5).

Fab1 and its regulators reside within a large protein complex

Coimmunoprecitation experiments were performed to test the model that Vac14p nucleates a large complex (Figure 2D). Using the tagged proteins Vac14p–HA and Vac14p–V5, we found that immunoprecipitation with anti-HA antibody coprecipitated Vac14p–V5 (Supplementary Figure S4A). Furthermore, Fab1p containing a C-terminal tandem affinity purification (TAP) tag (Fab1–TAP) coprecipitated Vac14p–V5 (Supplementary Figure S4B). Moreover, immunoprecipitation of Vac14p coprecipitates Fig4p (Supplementary Figure S4C). In addition, precipitation of Fig4p coprecipitates Fab1p (Supplementary Figure S4D). These interactions were reported independently (Rudge *et al*, 2004; Botelho *et al*, 2008), and it was proposed that Fab1p, Vac14p, and Fig4p form a ternary complex (Botelho *et al*, 2008).

Immunoprecipitation of Vac14p–Venus also coprecipitates Vac7p (Figure 2E). These coprecipitation experiments demonstrate that Vac14p interacts with itself, Fab1p, Fig4p, and Vac7p. We did not observe coprecipitation of Atg18p with Vac14p, Fab1p-TAP, or Vac7p (not shown).

To determine whether the proteins form a large complex, we used sedimentation analysis of detergent solubilized yeast cell lysates. When lysates were fractionated on a 10–50% glycerol gradient, Fab1 was distributed in two peaks (Figure 2F). The smaller peak, fraction 3, contained monomeric Fab1p (predicted molecular weight 257 kDa). The larger peak, fractions 6–8, contained Fab1p in a complex that sediments more slowly than the 670 kDa molecular weight standard in fractions 4 and 5. Although the predicted molecular weights of Vac7p, Fig4p, and Vac14p are 128, 101, and 99 kDa, respectively, significant proportions of these

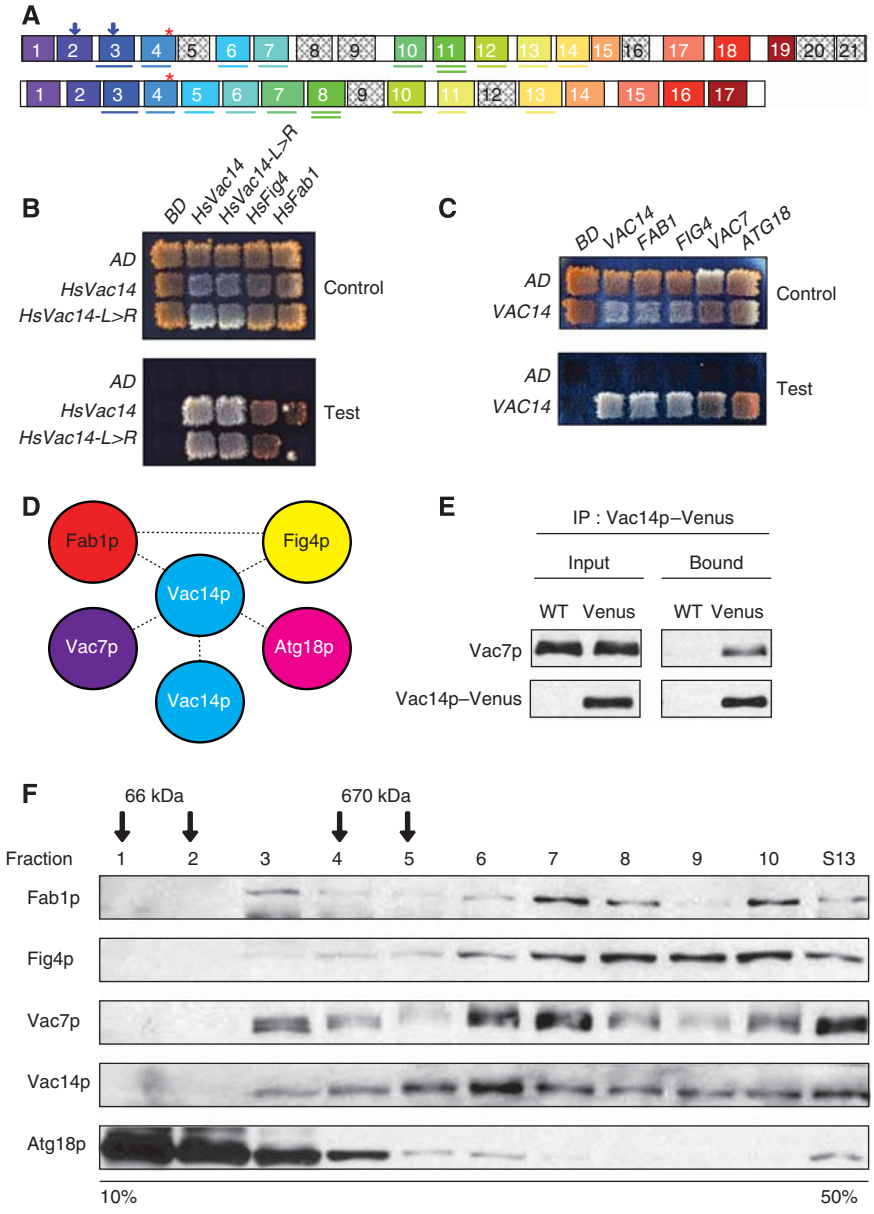

Figure 2 Vac14 nucleates the Fab1 complex. (**A**) Vac14 contains 21 and 17 HEAT repeats in *S. cerevisiae* (top) and mammalian Vac14 (bottom), respectively. Identical colours indicate homologous repeats between *S. cerevisiae* and mammalian Vac14. Red asterisk and blue arrows indicate *ingls* and *vac14-2* mutations, respectively. Underlines: HEAT repeats identified by REP with a confidence threshold better than at $P_0 < 1e{-}6$. (**B**) Yeast two-hybrid test of human Vac14 (HsVac14) or human Vac14–L156R (HsVac14-L>R), fused with the GAL4-activation domain (AD), interaction with itself, residues 346–1134 of human Fab1 or full-length Fig4, fused with the GAL4-binding domain (BD). Plasmids were cotransformed into the yeast cells and transformants were plated onto the SC-LEU-TRP plate and replica-plated onto SC-LEU-TRP (control) or SC-LEU-TRP-ADE-HIS plate (test). Plates were incubated at 24°C for 10 days. Growth on the test plate indicates protein–protein interaction. (**C**) Yeast two-hybrid test of Gal4-AD fused with yeast Vac14p tested with Gal4-BD fused with either Fab1p, Fig4p, Vac7p, Atg18p or Vac14p. Transformants were plated onto SC-LEU-TRP and replica-plated onto SC-LEU-TRP (control) or SC-LEU-TRP-ADE-HIS + 3AT (test). Plates were incubated at 24°C for 7 days. (**D**) Schematic of interactions between Fab1 and Fab1 regulators. (**E**) Vac14p–Venus coprecipitated Vac7p. Wild-type or *VAC14–Venus* cells were used. (**F**) Analysis on glycerol gradients (10–50%) indicate that Fab1p and regulators form a complex >670 kDa. Molecular weight markers bovine serum albumin, 66 kDa, and thyroglobulin, 670 kDa, run in an adjacent tube. Representative profile of two independent gradients. *vac14Δ/fig4Δ/ATG18–Venus* cells expressing pRS413–*VAC14–V5* and pRS415–*FIG4–Myc* were used.

proteins comigrated with the large Fab1p complex: Vac7p, in fractions 6 and 7; Fig4p, in fractions 6–8; and Vac14p, in fractions 5–8. That the peak fractions for Fab1p, Vac7p, Fig4p, and Vac14p overlap but are not identical may be explained by the presence of a mixture of partial and complete complexes. For example, the ternary complex of Fab1p, Vac14p, and Fig4p is found exclusively on the membrane of the vacuole, whereas Vac14p and Fig4p associate with each other in the cytosol (Botelho *et al*, 2008).

Most of the Atg18p (55 kDa) behaved as a monomer (fractions 1 and 2), but some Atg18p comigrated with the complex (fractions 5–7), suggesting that this small fraction is also part of the complex. Alternatively, the Atg18 in fraction 6 could be trailing from the earlier fractions. However, note that the intensity of fraction 6 is the same as fraction 5. Genetic evidence (below) strongly suggests that a portion of Atg18p is part of the Vac14p complex. Atg18p has a second distinct function in autophagy

and the large proportion of monomeric protein may be related to that function.

The above-mentioned results are consistent with the model that Vac14p nucleates a large complex containing Fab1p, Fig4p, Vac7p, Vac14p, and possibly Atg18p. Rather than pursuing analysis of the complex through further biochemical investigations, we identified and characterized mutations that partially disrupt the complex as a means to determine the functional significance of complete and partial complexes, and also map the interacting domains.

Fab1p, Vac14p, and Fig4p are required to form the core PI(3,5)P_2 regulatory complex

Fab1p does not interact with Fig4p in a yeast two-hybrid test. However, Fab1p–TAP coprecipitates with Fig4p, suggesting that the two proteins could interact indirectly. Indeed, co-precipitation of Fig4p by Fab1p–TAP required the presence of Vac14p and did not occur in the *vac14Δ* strain (Supplementary Figure S4E). Unexpectedly, coprecipitation of Fab1p–TAP with Vac14p required the presence of Fig4p (Supplementary Figure S4F). These data indicate that Fab1p requires both Vac14p and Fig4p to form a ternary complex *in vivo*. Localization experiments indicate that formation of the ternary complex is required for normal localization of members of the complex to the vacuole membrane (Figure 3A and B). Note that in each mutant, *vac14Δ*, *fig4Δ*, and *fab1Δ*, there is mislocalization to the cytoplasm of significant amounts of the remaining members of the complex.

Vac7p binds Vac14p in yeast two-hybrid and coimmunoprecipitation experiments (Figure 2C and 2E). To determine whether Vac7p is required for formation of the Fab1p/Vac14p/Fig4p complex, we carried out coprecipitation experiments in *vac7Δ* cells. Interaction of Fab1p with Vac14p (Supplementary Figure S6A) and Fig4p (Supplementary Figure S6B) did not require Vac7p. Localization of Fig4p, Vac14p, and Fab1p to the vacuolar membrane was independent of Vac7p (Supplementary Figure S6C). Similarly, Vac7p localization to the vacuole membrane is independent of Vac14p and Fig4p (Supplementary Figure S6C). Although two-hybrid studies support the proposal that Atg18p is part of the complex, this was not observed by coprecipitation. To further investigate the association of Atg18p with the complex, we examined the effects of Vac14p mutations (below).

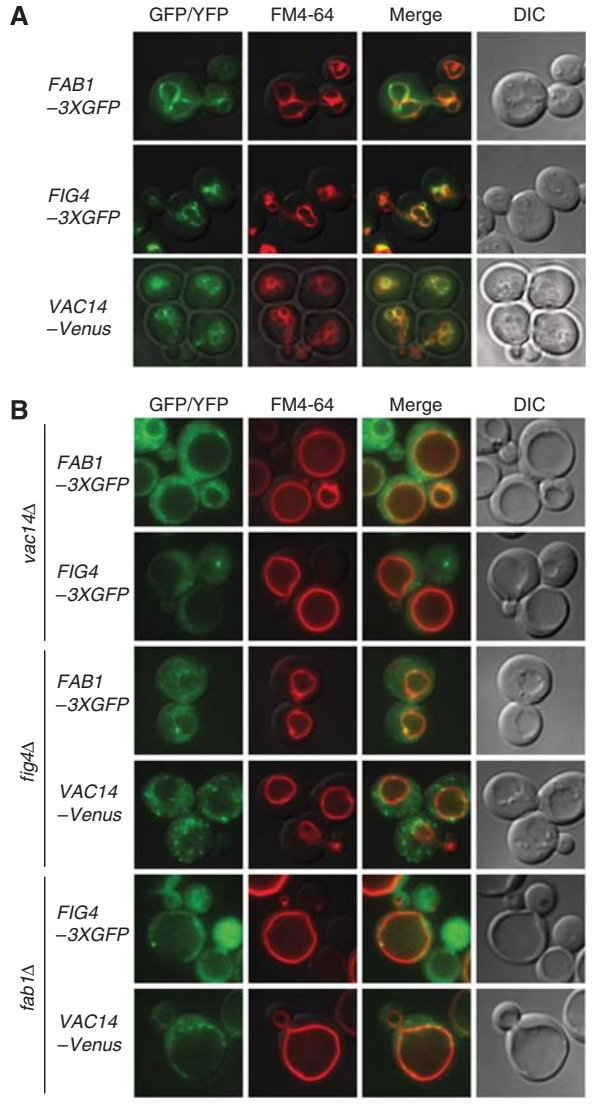

Figure 3 The localization of Fab1p, Fig4p, and Vac14p to the vacuole membrane requires the presence of all three proteins. Cells labelled with FM4-64 (red) to visualize the vacuole membrane. (**A**) Wild-type strains with *FAB1–3xGFP*, *FIG4–3xGFP*, or *VAC14–Venus* integrated at the proper chromosomal locus. (**B**) *FAB1–3xGFP* or *FIG4–3xGFP/vac14Δ* cells, *FAB1–3xGFP* or *VAC14–Venus/fig4Δ* cells and *FIG4–3xGFP* or *VAC14–Venus/fab1Δ* cells.

The Vac14–ingls mutation disrupts interaction with yeast Fab1p, Vac7p, and Atg18p

To further examine the molecular consequences of the *ingls Vac14–L156R* mutation, we generated the equivalent yeast mutant, *vac14–L149R*. The L149R mutation is located in HEAT repeat 4 (Figure 4A) and does not reduce protein stability (Figure 4B). The *vac14Δ* mutant has grossly enlarged vacuoles compared with the smaller and multilobed wild-type vacuoles (Figure 4C). When *vac14–L149R* is present as the sole copy of *VAC14*, vacuole size and morphology are intermediate between the multilobed wild-type and the *vac14Δ* mutant, consistent with partial loss of function (Figure 4C).

In a yeast two-hybrid test, vac14p–L149R was defective in binding Fab1p, Vac7p, and Atg18p, although retaining normal interaction with Fig4p and with itself (Figure 4D). vac14p–L149R also failed to coprecipitate with Fab1p–TAP (Figure 4E). In the presence of vac14p–L149R, Fab1p did not localize to the vacuole membrane (Figure 4F). Thus, HEAT repeat 4 is critical for the interaction between Vac14p and Fab1p and is required for the intracellular localization of Fab1p.

In contrast, vac14p–L149R did coprecipitate with Fig4p and with itself (Supplementary Figure S7), indicating that the Fig4p and Vac14p interaction domains are located in a different region of Vac14p from the L149 mutation.

To examine the effect of loss of Fab1p from the PI(3,5)P_2 regulatory complex, we examined the *in vivo* levels of PI(3,5)P_2. Under basal conditions, PI(3,5)P_2 comprises approximately 0.04% of total PI lipid in the *vac14Δ* strain expressing wild-type *VAC14* from a plasmid. When cells are exposed to hyperosmotic stress, PI(3,5)P_2 increases 10-fold to approximately 0.5% of total PI lipid within 10 min, then decreases to 0.3% at 20 min, and to 0.09% at 30 min

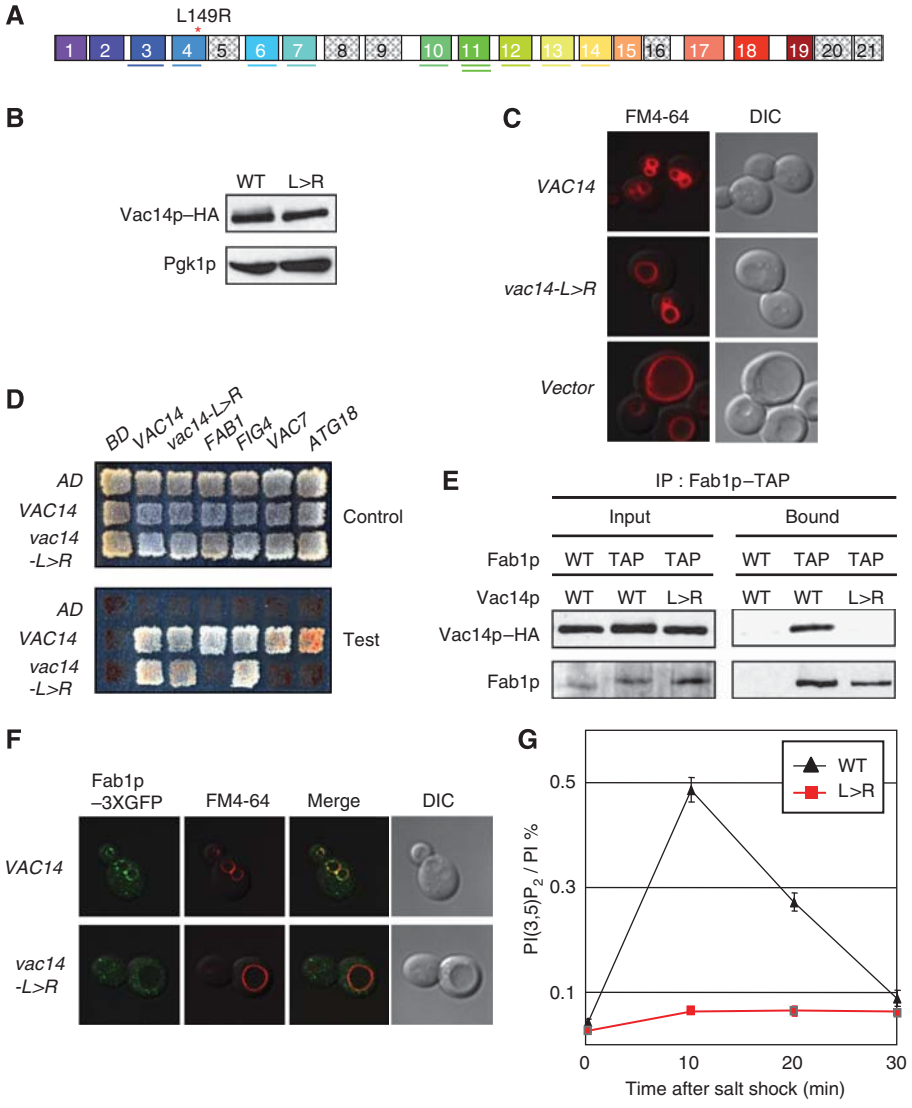

Figure 4 The vac14–L149R mutant is defective in its association with Fab1p. (**A**) Schematic of the *vac14–L149R* mutant. Red asterisk: mutation site. (**B**) vac14–L149R protein is stable. Cell lysates from a *vac14Δ* strain expressing pRS413–*VAC14-HA* or pRS413–*vac14–L149R–HA* (L>R) analysed by western blot. Vac14p detected with anti-HA antibody. Loading control: Pgk1. (**C**) *vac14–L149R* mutant retains partial function. Vacuoles in the *vac14–L149R* mutant are intermediate in size between *vac14Δ* and wild-type vacuoles. Vacuoles visualized with FM4-64 (red). *vac14Δ* strain transformed with pRS413–*VAC14*, pRS413–*vac14–L149R* (*vac14-L>R*), or pRS413 (vector). (**D**) Yeast two-hybrid test of Vac14p or vac14p–L149R interaction with itself, Fab1p, Fig4p, Vac7p, and Atg18p. Full-length Vac14p or vac14p–L149R (*vac14-L>R*) fused with Gal4-AD and Gal4-BD. Full-length Fig4p; Atg18p; amino acids 394–918 of Vac7p, amino acids 538–1085 of Fab1p, fused with Gal4-BD. Upper panel, SC-LEU-TRP (control); lower panel, SD-LEU-TRP-ADE-HIS + 3AT (test). (**E**) Pull-down of Fab1p–TAP coprecipitates wild-type Vac14p, but not vac14p–L149R. Detergent-solubilized extracts from a *vac14Δ* or *vac14Δ/FAB1–TAP* strain expressing pRS413–*VAC14–HA* (WT), or pRS413–*vac14–L149R–HA* (*L>R*). Vac14p but not vac14p–L149R binds Fab1p–TAP IgG beads. (**F**) Fab1p localization is defective in the vac14p–L149R mutant. A *vac14Δ/FAB1–3XGFP* strain transformed with pRS413–*VAC14* or pRS413–*vac14–L149R* (*vac14-L>R*). FM4-64 (red), Fab1p–3xGFP (green). (**G**) The *vac14–L149R* mutant does not increase its levels of $PI(3,5)P_2$ in response to hyperosmotic stress. *vac14Δ* cells expressing pRS413–*VAC14* or pRS413–*vac14–L149R* were labelled with [^{3}H]inositol for 16 h and exposed to 0.9 M NaCl for times indicated. Values are the percentage of total extracted [^{3}H]PI. Error bars: s.d. ($n = 3$).

(Figure 4G, Supplementary Table S1). (The 10-fold increase in this wild-type strain compared with a more typical 20-fold increase may be a consequence of the expression of *VAC14* from a plasmid rather than from its chromosomal location.) In the *vac14Δ* strain expressing *vac14–L149R*, $PI(3,5)P_2$ comprises 0.03% of the PI lipid under basal conditions and increases only two-fold to 0.06% after 10 min of hyperosmotic stress. Thus, dissociation of Fab1p from the complex through loss of interaction between Vac14p and Fab1p results in defective activation of Fab1 lipid kinase activity in response to hyperosmotic shock. That the modest increase in $PI(3,5)P_2$ is sustained for at least 30 min suggests that regulation of Fig4p lipid phosphatase activity may also be impaired by the loss of association of Fab1p and Vac14p.

The fab1-2 mutant reveals that activation of Fab1p requires its association with the Vac14p complex

We sought to identify a mutation in Fab1p that disrupted its interaction with Vac14p, and found that the *fab1-2* mutant (Yamamoto *et al*, 1995) is specifically defective in this interaction. We sequenced the mutant *fab1-2*, and identified a single missense mutation, G864E, in the CCT domain

(Figure 5A). The mutant protein is stable *in vivo* (Figure 5B) and retains normal kinase activity *in vitro* (Supplementary Figure S8). The CCT domain of Fab1p shares homology with the GroEL and the CCT family of Hsp60 chaperones, suggesting that it could be involved in protein–protein interactions. The G864E mutation is located within Fab1p peptide 538–1085, which interacts with Vac14p in a yeast two-hybrid test (Figure 2C and 5C). We therefore tested the effect of this mutation on the interaction between Fab1 and Vac14. In the yeast two-hybrid test, *fab1–G864E* does not interact with *VAC14* (Figure 5C). Wild-type Fab1p coimmunoprecipitates with Vac14p–Venus, but the Fab1p–G864E mutant does not (Figure 5D). Thus, the G864E mutation disrupts interaction of Fab1p with Vac14p.

Fab1p coimmunoprecipitates with Fig4p–3XGFP (Figure 5E). However, the Fab1p–G864E mutant protein does not coprecipitate with Fig4p–3XGFP (Figure 5E). This further supports the model that interaction of Fab1p with

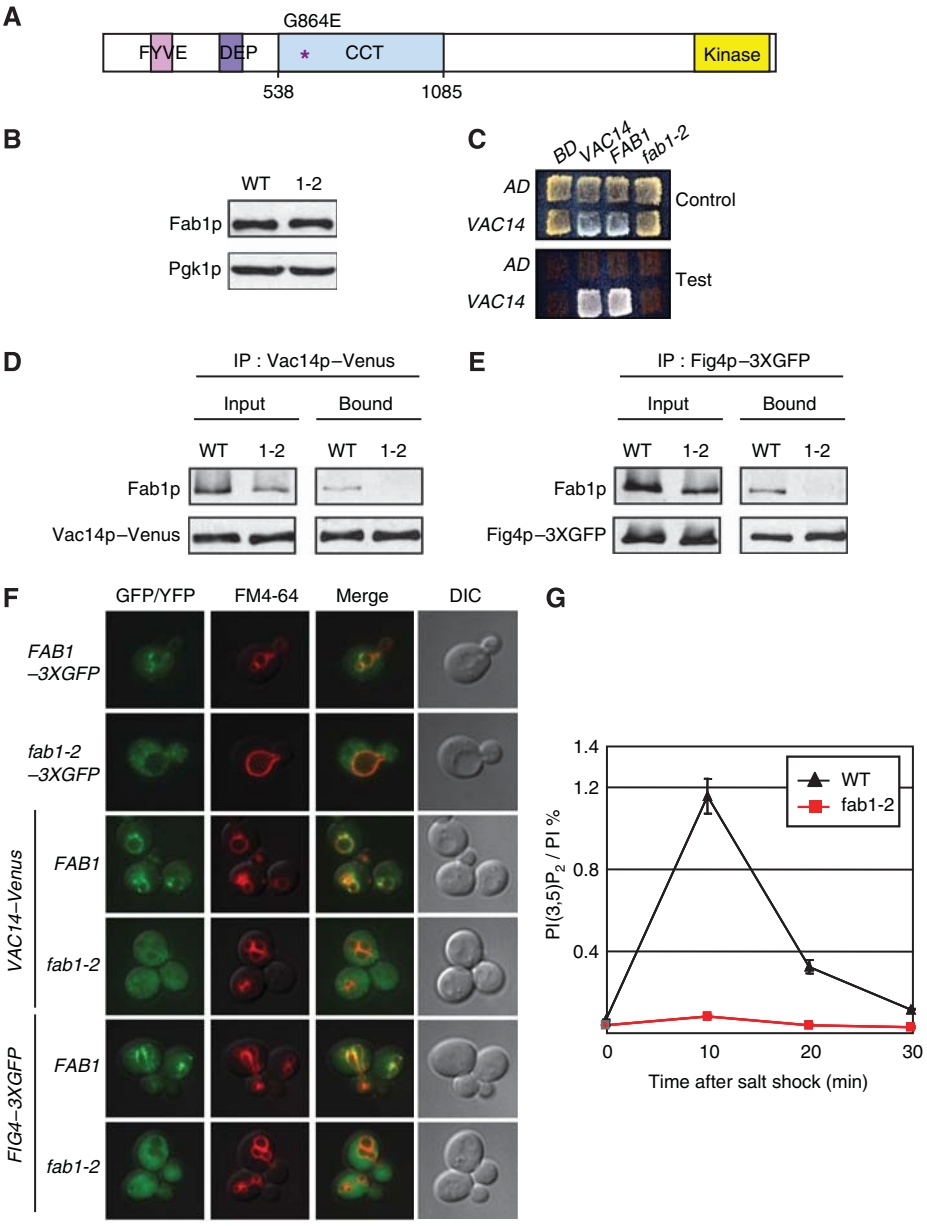

Figure 5 Formation of a ternary complex of Fab1p, Vac14p, and Fig4p is required for Fab1p kinase activity *in vivo*. (**A**) Schematic of the *fab1-2* allele; purple asterisk, the G864E mutation. (**B**) Fab1-2 protein is present at wild-type levels. Cell lysates analysed by western blot analysis from *fab1Δ* cells expressing pRS416–*FAB1* or pRS416–*fab1-2*. Equal protein loaded. (**C**) *VAC14* interacts with *FAB1*, but not *fab1-2*. Yeast two-hybrid test of *FAB1* or *fab1-2* interaction with *VAC14*. Full-length *VAC14* fused with Gal4-AD. *FAB1* or *fab1-2*, amino acids 538-1085. fused with Gal4-BD. Upper panel, SC-LEU -TRP (control); lower panel, SC-LEU-TRP-ADE-HIS + 3AT (test). Plates incubated at 24°C for 4 days. (**D–E**) fab1-2 does not form a complex with Vac14p and Fig4p. (D) Vac14p–Venus does not coprecipitate fab1-2. pRS416–*FAB1* or pRS416–*fab1-2* expressed in a *fab1Δ/VAC14–Venus* strain. (E) fig4p–3xGFP does not coprecipitate fab1-2. pRS416–*FAB1* or pRS416–*fab1-2* expressed in a *fab1Δ/FIG4–3xGFP* strain. (**F**) fab1-2, Vac14p and Fig4p in a *fab1-2* mutant do not localize to the vacuole membrane. pRS416–*FAB1–3xGFP* or pRS416–*fab1-2–3xGFP* expressed in *fab1Δ*, or *fab1Δ/VAC14–Venus* or *fab1Δ/FIG4–3xGFP*. Cells labelled with FM4-64 (red). (**G**) The *fab1-2* mutant does not transiently increase its levels of $PI(3,5)P_2$ in response to hyperosmotic stress. *fab1Δ* cells expressing pRS416–*FAB1* or pRS416–*fab1-2* measured as described in Figure 4. Error bars: s.d. ($n = 3$).

Fig4p is dependent on interaction of Fab1p and Fig4p with Vac14p (Supplementary Figure S4E and F). These coprecipitation results are similar to those observed for fab1p–T1017I, another point mutation in the CCT domain (Botelho *et al*, 2008).

The fab1-2 mutant protein fails to localize to the vacuole membrane (Figure 5F). Localizations of Vac14p–Venus and Fig4p–3xGFP to the vacuole membrane are also defective in the presence of fab1-2 protein (Figure 5F). Formation of the ternary complex thus appears to be required for correct localization of each component.

To determine the importance of formation of the ternary complex for the hyperosmotic stress-induced activation of Fab1p, we tested the effect of osmotic stress on $PI(3,5)P_2$ levels in the *fab1-2* mutant. In the wild-type strain, the basal levels of $PI(3,5)P_2$, 0.05% of total PI lipid, increase 20-fold to 1.15% within 10 min after hyperosmotic stress, then decrease to 0.32% at 20 min and 0.11% at 30 min (Figure 5G, Supplementary Table S1). In the *fab1-2* mutant, the basal levels of $PI(3,5)P_2$, 0.033%, increased only two-fold after 10 min, similar to the *vac14–L149* mutant described above. These data support the conclusion that association with the complex is required for the hyperosmotic stress-induced activation of Fab1p and for the physiological regulation of $PI(3,5)P_2$ levels.

The vac14-2 mutant disrupts interaction with Vac7p and Atg18p and results in defective activation and inhibition of Fab1p

Vac7p is a major activator of yeast Fab1p, and basal levels of $PI(3,5)P_2$ are significantly reduced in a *vac7Δ* mutant, resulting in enlarged vacuoles (Bonangelino *et al*, 1997; Duex *et al*, 2006b). We screened for gain-of-function mutations of Vac14p that could rescue the low levels of $PI(3,5)P_2$ and reduce the enlarged vacuoles in *vac7Δ* cells. Random PCR mutagenesis of *VAC14* was performed and the mutants were transformed into a *vac14Δ, vac7Δ* strain. Mutants that restored growth at 37°C and partially corrected the enlarged vacuoles were isolated. When the strongest of these mutants, *vac14-2*, was expressed in a *vac14Δ* strain, vacuole size was smaller than in wild-type cells (Figure 6A), suggesting that $PI(3,5)P_2$ level is increased in this mutant. Direct measurement demonstrated a two-fold increase of the basal level of $PI(3,5)P_2$ in the *vac14-2* mutant (Figure 6B, Supplementary

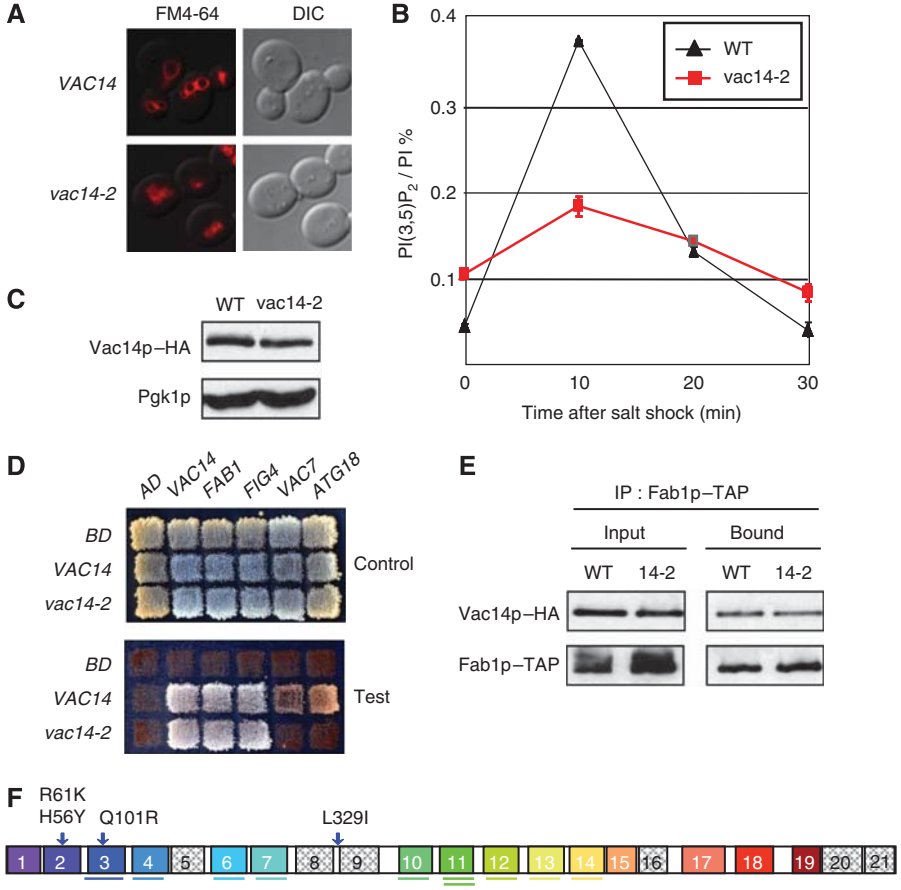

Figure 6 Vac7p and Atg18p function through Vac14p. (**A**) *vac14-2* has smaller than normal vacuoles, consistent with elevated basal levels of $PI(3,5)P_2$. *vac14Δ* cells expressing pRS416–*VAC14* or pRS416–*vac14-2* labelled with FM4-64. (**B**) *vac14-2* has higher basal levels of $PI(3,5)P_2$, but does not elevate or turnover $PI(3,5)P_2$ during osmotic stress. $PI(3,5)P_2$ levels in *vac14Δ* cells expressing pRS416–*VAC14* or pRS416–*vac14-2* measured as described in Figure 4. Error bars: s.d. ($n=3$). (**C**) vac14-2 protein is present at wild-type levels. Cell lysates analysed by western blot analysis from *vac14Δ* cells expressing pRS413–*VAC14–HA* (WT) or pRS413–*vac14-2–HA(14-2)*. Pgk1p: loading control. (**D**) Vac14-2 is defective in binding Vac7p and Atg18p. Yeast two-hybrid test of *VAC14* or *vac14-2*, fused with Gal4-AD, interaction with *FAB1*, *FIG4*, *VAC7*, *ATG18*, fused with Gal4-BD. Upper panel, SC-LEU-TRP (control); lower panel: SC-LEU-TRP-ADE-HIS +3AT (test). Plates incubated at 24°C, 7 days. (**E**) Fab1p coprecipitates vac14-2. Detergent-solubilized extracts from a *vac14Δ* or *vac14Δ/FAB1–TAP* strain expressing pRS413–*VAC14–HA* (WT), or pRS413–*vac14-2–HA* (14-2). (**F**) Schematic of the *vac14-2* allele; blue arrows indicate the mutation sites.

Table S1). However, when the *vac14-2* mutant was treated with hyperosmotic stress, the level of $PI(3,5)P_2$ increased only 1.7-fold, compared with an 8-fold increase in the wild-type strain (Figure 6B). There was no change in the steady-state level of vac14-2 protein compared with wild type (Figure 6C). The abnormal regulation of $PI(3,5)P_2$ thus appears to be caused by altered function of the vac14-2 protein.

In a yeast two-hybrid test, *vac14 -2* is specifically defective in interaction with Vac7p and Atg18p (Figure 6D). Interaction of vac14-2 protein with Vac14p, Fig4p, and Fab1p is normal and formation of the ternary complex is unaffected. The vac14-2 protein also coprecipitates Fab1p to the same extent as wild-type Vac14p (Figure 6E).

vac14-2 contains four mutations: H56Y, R61K, Q101R, and L329I (Figure 6F). Three of these mutations, H56, R61, and Q101, are located in HEAT repeat loops 2 and 3. These residues exhibit evolutionary conservation. Tested singly in a yeast two-hybrid test, each mutation perturbed the interaction of Vac14p with Vac7p and Atg18p, without disrupting interaction with its other binding partners (not shown). Thus all three residues are important for Vac14p interaction with Vac7p and Atg18p. L329 alone had no effect on the interaction of Vac14p with its known binding partners (data not shown). These results indicate that HEAT repeats 2 and 3 directly contact Vac7p and Atg18p, but do not contact Fab1.

The elevation in basal levels of $PI(3,5)P_2$ in the *vac14-2* mutant is consistent with the model that negative regulation of Fab1p by Atg18p requires binding of Atg18p to Vac14p. Whereas the yeast two-hybrid test detected interaction of Atg18p with Vac14p, this was not observed in pull-down experiments. Thus, it is informative that a mutation in Vac14p that interrupts its ability to interact with Atg18p also results in $PI(3,5)P_2$ levels that are consistent with a partial release of Atg18p inhibition of Fab1p. The *vac14-2* mutant provides additional support for the hypothesis that Atg18p interacts with Vac14p.

The *vac14-2* defect in osmotic stress-induced elevation of $PI(3,5)P_2$ supports the model that Vac7p, a positive regulator of Fab1p, exert an effect through binding to Vac14p. The association of Vac7p with wild-type Vac14p was demonstrated in the yeast two-hybrid test and by coimmunoprecipitation (Figure 2C, E).

The Fig4p-binding site on Vac14p is distinct from the Fab1p-, Vac7p-, and Atg18p-binding sites

Fab1p and Vac7p bind near the N terminus of Vac14p. On the basis of the predicted HEAT motifs of Vac14p, we divided the protein into two overlapping constructs (Figure 7). HEAT repeats 1–10 interact with Fab1p and Vac7p but not with Fig4p. HEAT repeats 10–21 interact only with Fig4p. These results demonstrate that Fab1p and Vac7p bind to the N-terminal half of Vac14p, whereas Fig4p binds to a distinct site in the C-terminal half. Atg18p binds full-length Vac14p but does not bind to either half of the molecule. On the basis of the vac14-2 mutant, we predict that contact points for Atg18p include the intrarepeat loops of HEAT repeats 2 and 3.

Discussion

Here, we present support for the model that Fab1, Vac14, and Fig4 form a ternary complex. While this article was in preparation, independent evidence for formation of this complex in yeast was reported (Botelho *et al*, 2008). Our present studies significantly extend those studies by our discovery that the complex is nucleated by Vac14. Moreover, analysis of the new, partially functional *fab1* and *vac14* mutants demonstrate that the yeast complex includes

Figure 7 Yeast two-hybrid analysis of the minimal region of Vac14p required for interaction with Fab1p, Fig4p, Vac7p, and Atg18p. Lines above the schematic indicate the minimal region of Vac14p required for binding with each protein. Full-length *VAC14* or truncated *VAC14* was fused with Gal4-AD. *FAB1* encoding amino acids 538–1085, *VAC7* encoding amino acids 394–918: full-length *ATG18* or *FIG4* was fused with the BD. Lines below the schematic indicate the regions of Vac14p tested.

Vac7p, a positive regulator of Fab1p, and is most likely to include Atg18p, an inhibitor of Fab1p. We find that both Vac7p and Atg18p exert an effect through direct contact with Vac14p. Our analysis strongly suggests that the organization of the complex produces dynamic, stimulus-induced changes in $PI(3,5)P_2$, by three distinct mechanisms. First, the activator Vac7p and the inhibitor Atg18p bind to overlapping sites, close to the site of Fab1p. This arrangement could facilitate the rapid activation and inactivation of the Fab1p lipid kinase during hyperosmotic stress in yeast. Second, Fab1p and Fig4p bind simultaneously to nonoverlapping sites on Vac14p, bring them into close proximity, so that the lipid kinase and phosphatase share access to the same pools of PI3P and $PI(3,5)P_2$. Third, the close proximity of Fab1p and Fig4p is also consistent with our earlier postulate that Fig4p may function as a protein phosphatase to activate Fab1p by dephosphorylation (Duex *et al*, 2006b).

Vac14 contains multiple HEAT repeats

The partial loss of function of Vac14 in the *ingls* mouse prompted us to evaluate the molecular function of this uncharacterized protein. Our bioinformatics analysis predicted that both the yeast and mammalian Vac14 proteins are composed entirely of HEAT repeats. Tandem HEAT repeats form a super-helical structure that provides docking sites for other proteins. The most common protein–protein docking sites are the intrarepeat loops (Groves *et al*, 1999; Xing *et al*, 2006). Three point mutations in *vac14-2* that impair protein interaction are located in predicted intrarepeat loops, R61K and H56Y in HEAT 2 and Q101R in HEAT 3. The location in the intrarepeat loops of three, random independent mutations that alter protein interactions supports the prediction of the HEAT repeat structure of Vac14. Analysis of the vac14-2 mutant also indicates that Vac7p and Atg18p bind overlapping sites that include the intrarepeat loops of HEAT repeats 2 and 3.

A second potential protein–protein interaction site is on a face formed by the B helices of HEAT repeats (Chook and Blobel, 1999; Cingolani *et al*, 1999). The helices provide both structure and points of protein–protein contact. The *ingls* mutation is located on the predicted B helix of HEAT 4. This mutation affects the binding of Fab1p and also impairs binding of Atg18p and Vac7p. The Fab1p-, Atg18p-, and Vac7p-binding sites may overlap, or the vac14–L149R mutation may perturb the surrounding structure, altering the Fab1p-binding site and a separate Atg18p/Vac7p-binding site. The overlap of Atg18p and Vac7p sites at a position close to the Fab1p-binding site is consistent with competitive regulation of Fab1p by its positive and negative regulators.

Vac14 is a scaffold for the Fab1 kinase complex

As HEAT repeats mediate protein–protein interactions, we investigated and found that Vac14p nucleates the assembly of a complex containing the proteins that synthesize and turn over $PI(3,5)P_2$. The location of the *vac14–L149R* and *vac14-2* mutations near the N-terminal region of Vac14p indicates that the N-terminal half of Vac14p binds Fab1p, Vac7p, and Atg18p. Indeed, in a yeast two-hybrid test, HEAT repeats 1–10 of Vac14p were sufficient to bind Fab1p and Vac7p (Figure 7). Conversely, HEAT repeats 10–21 of Vac14p were sufficient to bind Fig4p (Figure 7). Thus, Fab1p, Fig4p, and two additional Fab1p regulatory proteins all directly contact Vac14p and make a large complex that regulates both the synthesis and turnover of $PI(3,5)P_2$.

The composition of the PI(3,5)P_2 regulatory complex facilitates dynamic regulation of PI(3,5)P_2

The *fab1-2* mutation disrupts the ability of Fab1p to interact with Vac14p and prevents coprecipitation of Fab1p with Fig4p. Negative two-hybrid test results (not shown) suggest that Fab1p and Fig4p do not interact directly. Fab1p binds to the N terminus and Fig4p binds to the C terminus of Vac14p. We propose that Vac14p assumes a conformation that brings Fab1p into close proximity to Fig4p (Figure 8). This physical proximity may explain our previous evidence that the lipid phosphatase Fig4p is an activator of the Fab1p kinase, possibly through dephosphorylation of the Fab1 protein. Importantly, the phosphatase activity of Fig4p is required for its regulatory function; an active site mutant that retains interaction with Vac14p is nonetheless defective in elevation of $PI(3,5)P_2$ levels (Bonangelino *et al*, 1997; Duex *et al*, 2006b). Fig4p may also contribute to Fab1p activation through stabilization of the regulatory complex.

In addition to both the lipid phosphatase and lipid kinase, the $PI(3,5)P_2$ regulatory complex includes a second pair of proteins with opposing effects on $PI(3,5)P_2$ levels: a lipid kinase activator and inhibitor. The close association of each of these proteins in a complex may be key to the rapid modulation of $PI(3,5)P_2$ levels *in vivo* (Duex *et al*, 2006a).

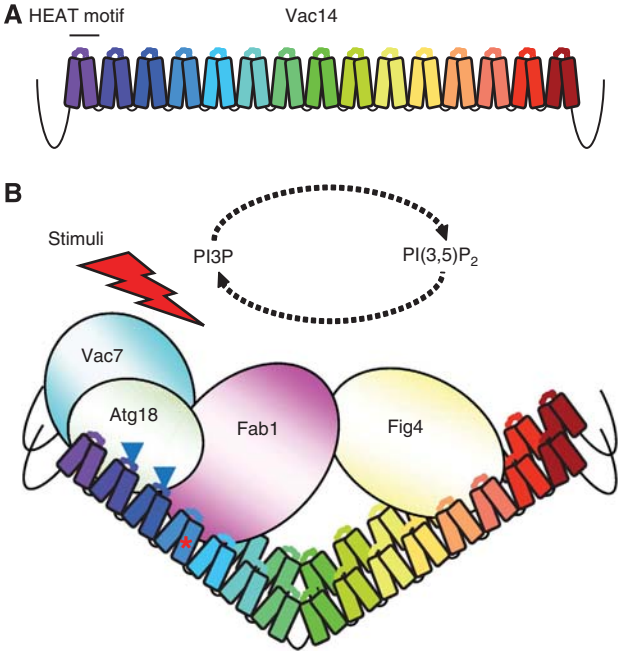

Figure 8 Model of the Vac14 complex. (**A**) Schematic Vac14. (**B**) Vac14p binds to both Fab1p and Fig4p and may undergo a conformational change that brings Fab1p into contact with Fig4p. Fig4p functions as both an activator of Fab1p and a $PI(3,5)P_2$ 5-phosphatase. Fig4p and Fab1p bind to distinct regions on Vac14p. The Fab1p-binding site significantly overlaps with Vac7p- and Atg18p-binding sites. Blue arrowheads indicate the vac14-2 mutations sites, the arrow to the left indicates the location of H56Y and R61K, the arrow to the right marks Q101R. These arrows show the region of Vac14p that contacts Vac7p and Atg18p. Red asterisk indicates the *vac14-ingls* mutation, which disrupts interaction with Fab1p, Vac7p, and Atg18p.

Identification of the components of the Vac14p complex provides new insights into the acute regulation of $PI(3,5)P_2$ levels. First, the Fab1p lipid kinase and Fig4p lipid phosphatase reside in the same complex and bind to opposite ends of Vac14p. A conformational change in Vac14p could simultaneously affect the activities of the kinase and phosphatase in opposite directions, amplifying the net effect on $PI(3,5)P_2$. Second, the complex contains both an activator and an inhibitor of Fab1p, Vac7p, and Atg18p, respectively, which bind to the same region of Vac14p, and most likely bind close to Fab1p. Again, an altered conformation of Vac14p could result in opposite effects on binding of the two proteins, amplifying the effect of either one alone on Fab1p activity. Third, Fig4p has a dual function and is both a lipid phosphatase and an activator of the lipid kinase. The structure of the protein complex is most likely to facilitate the rapid flux in $PI(3,5)P_2$ levels that occurs in response to various biological stimuli.

PI(3,5)P_2 is required for neural function and pigmentation

Similar to the null mutations of mouse *Fig4* and *Vac14* (Chow *et al*, 2007; Zhang *et al*, 2007), the *Vac14–ingls* mutation results in reduced intracellular levels of $PI(3,5)P_2$, cytoplasmic vacuolization, neurodegeneration, and early lethality. As the *Vac14*-null mouse dies perinatally, defects in nervous system function were inferred solely from the histopathology of newborn mice. The *ingls* mouse lives up to 3 weeks, permitting direct observation of abnormal neurological function, pigmentation, and growth defects. The *Vac14*–ingls mice develop a tremor and motor incoordination exemplified by ataxic gait and difficulty in righting. Although the steady-state levels of Vac14–ingls protein are normal and interaction with Fig4 is retained, binding of Fab1 is abolished. The failure of the corresponding yeast mutant to activate Fab1 strongly suggests that failure of *ingls* Vac14–L156R to activate mammalian Fab1 accounts for the low level of $PI(3,5)P_2$ in fibroblasts from the *ingls* mouse. The data suggest that dissociation of Fab1 from the $PI(3,5)P_2$ regulatory complex is the molecular basis for neurodegeneration and lethality in the *ingls* mouse. Thus, the ability of Vac14 to nucleate the complete $PI(3,5)P_2$ regulatory complex is essential for normal neural function.

Differences between the *Vac14*–ingls, *Vac14*-null and *Fig4*-null mice are listed in Supplementary Table S2. DRG neurons are severely affected in the *Fig4*- and *Vac14*-null mice, but are spared in the *Vac14–ingls* mutant. This rescue of sensory neurons may be explained by their greater capacity for synthesis of $PI(3,5)P_2$, or by a higher abundance of downstream effector proteins. The *Vac14–ingls* mutant exhibits astrocytosis with earlier onset and greater severity than the other mutants, which merits further investigation. Hydrocephalus is also more severe in the *ingls* mice, with huge distention of the ventricles. Differences in the abundance of interacting proteins may account for the cell-type-specific effects of these mutations. The mixed-strain backgrounds of the two null mutants may also contribute to phenotypic differences from the congenic C57BL/6J.ingls mice discussed here.

Defects of PI(3,5)P_2 regulation and human disease

Mutations of human *FIG4* result in the peripheral neuropathy Charcot–Marie–Tooth type 4J, with features similar to those in the *Fig4*-null mouse (Chow *et al*, 2007). To determine whether mutations of *Vac14* could contribute to Charcot–Marie–Tooth disorder, we screened the previously described cohort of 95 patients for variants of *VAC14*. No variants in coding sequence or splice sites of *VAC14* were observed (C Chow, M Meisler, M Khajavi, K Szigeti and JR Lupski, unpublished data). We also investigated the function of *VAC14* in the human neurological disorder *SCA4*, which maps to a region of chromosome 16q22 that contains the *VAC14* gene (Flanigan *et al*, 1996). We sequenced the exons of *VAC14* in an affected member of the original *SCA4* family, but did not detect any coding or splice site mutations (C Chow, M Meisler, and Y-H Fu, unpublished data). Thus, the contribution of *VAC14* mutations to human disease remains unknown. Extensive gliosis in patients with Alexander disease is caused by mutation of *GFAP*; it is possible that *VAC14* or *FIG4* could contribute to other disorders characterized by gliosis. The lack of DRG defects in the *ingls* mice, in contrast to the previously described null mutants, suggests that *VAC14* could have an important function in human neurological disorders that are restricted to the CNS and have not yet been tested.

Evolutionary conservation of PI(3,5)P_2 regulation

Our study used the cognate mutation in yeast to provide molecular insight into the pathology of the *ingls* mouse. This work indicates that the activation of Fab1 by the Vac14 complex is conserved from yeast to mammals and is essential for nervous tissue function, pigmentation and viability. Vac14 nucleates assembly of the $PI(3,5)P_2$ core regulatory complex in yeast and serves as a scaffold for the complex (Figure 8). Loss of interaction between Vac14 and Fab1 results in the lethal neurological disorder in *ingls* mice. Analysis of the *ingls* mutation enabled us to localize the Fab1-interaction domain of Vac14. In yeast, the *vac14–ingls* mutation also disrupts interaction with Vac7p, a positive regulator of Fab1p, and Atg18p, a negative regulator. The mammalian homologue of Vac7p has not been identified, whereas four distinct homologues of Atg18p are present in the mammalian genome: WIPI 1–4. Further work will be required to identify all components of the mammalian $PI(3,5)P_2$ regulatory complex and to determine the functions of $PI(3,5)P_2$. Thus far, we have described pathological mutations in the core components *Fig4* and *Vac14* (Chow *et al*, 2007; Zhang *et al*, 2007; this article). Heterozygous mutations of human *FAB1* cause the mild eye phenotype corneal fleck dystrophy (OMIM 609414). In view of the vulnerability of neurons to alteration of $PI(3,5)P_2$ levels, mutations in other components of the $PI(3,5)P_2$ regulatory complex are likely to contribute to human neurological disease.

Materials and methods

Animals

The *ingls* mutation arose at The Jackson Laboratory in 1991 on the inbred strain DBA/2J and is maintained as a congenic line on the C57BL/6J background (current generation F23). Mice are available from the Jackson laboratory as B6.D2-ingls/J (stock 003095). Preliminary description of the mutant and its location on chromosome 8 was submitted to the Jackson Laboratory website (Bronson *et al*, 2003). The *Vac14*$^{\beta-geo}$ line was generated from a gene-trap ES cell from strain 129/Ola, and it lacks detectable protein (Zhang *et al*, 2007). The gene-trap mice were first crossed to strain C57BL/6J and

the *Vac14*$^{\beta-geo}$ mutant has been maintained as a mixed stock (C57BL/6J X 129/Ola)F12, by mating heterozygotes.

Genotyping

SNP1, CTC AAA CTT CAC CCC (C/T) AGC CCC ACC CCA ACC, is located at nucleotide 111,611,180 of mouse chromosome 8 (Mouse Build 37.1, www.ensembl.org) and was genotyped at Kbiosciences (www.kbioscience.co.uk/software/snpviewer). Mouse *Vac14* exon 4 containing the *ingls* mutation is amplified with the following primer pair, designated as Vac14E4: forward, 5′CAG CCA GTG GGA ACA ACC GTG TGA; and reverse, 5′ ACA TAG ACA TGC AAG CAG GCA AAG. These primers are used for genotyping the L156R mutation by virtue of the loss of a *Sac*I site in the mutant allele (Figure 1B).

Histology

Tissues were sectioned and stained with H&E at HistoServ (Germantown, MD). For GFAP staining, mice were perfused with 4% paraformaldehyde, and tissues were sectioned and stained as described (Liu *et al*, 2007). Twenty-micrometer cryostat sections were stained with anti-GFAP (1:1000, rabbit polyclonal, Sigma) and with secondary antibodies conjugated with biotin (1:200, Vector Laboratory, Burlingame, CA) followed by avidin–biotin complex (1:50, Elite, Vector Laboratory). Immunoreactivity was visualized with diaminobenzidine and 0.02% hydrogen peroxide for up to 5 min.

Western blot

For mouse samples, dissected brain cortex was homogenized in 150 mM NaCl, 1.0% NP-40, 0.5% deoxycholate, 0.1% SDS, 1 mM EDTA, 50 mM Tris–HCl, pH 8.0, with protease inhibitors; Roche (Cat. no. 11 873 580 001), and lysed on ice for 1 h. Molecular weight markers; Amersham (cat. no. RPN7567). Anti-Vac14 antibody (Zhang *et al*, 2007). For yeast samples, experiments were performed as described previously (Duex *et al*, 2006b).

Phosphoinositides and vacuoles in cultured cells and yeast cells

For cultured cells, primary fibroblasts were starved in inositol-free DMEM 12 h and labelled with myo-[2-^{3}H]inositol, 36 h. Lipids were extracted, deacylated, and analysed by anion-exchange HPLC chromatography (Zhang *et al*, 2007). Images of cells were taken on an Axioscope 2 (Carl Zeiss MicroImaging, Jena, Germany) using a LUCPlanFL N $\times$40/0.60 Ph2 objective with a DeltaVision microscope system. For yeast cells, experiments were performed as described previously (Duex *et al*, 2006b).

Prediction of HEAT repeat motifs

Seventeen Vac14 sequences analysed were from: *S. cerevisiae* (NP_013490.1); *Ashbya gossypii* ATCC 10895 (NP_984909); *Aspergillus fumigatus* Af293 (XP_751167.1); *Kluyveromyces lactis* (XP_454179.1); *Yarrowia lipolytica* (XP_501232.1); *Gibberella zeae* PH-1 (XP_390022.1); *Candida glabrata* (XP_447078.1); *Ustilago maydis* 521(XP_757421.1); *Candida albicans* SC5314 (XP_716167.1); *Neurospora crassa* OR74A (XP_959537.1); *Debaryomyces hansenii* CBS767 (XP_456837.1); *S. pombe* 972 h (NP_596363.1); *Cryptococcus var. neoformans* B-3501A (XP_775858.1); *Homo sapiens* (NP_060522.3); *Caenorhabditis elegans* (NP_492215); *D. melanogaster* (NP_650208); *Arabidopsis thaliana* (NP_565275). Potential HEAT repeats in each sequence are identified using REP without an applied confidence threshold. Regions of *S. cerevisiae* Vac14 with homology to the predicted HEAT repeat in other species were assumed to form HEAT repeats. The resulting repeats were further analysed by the secondary structure prediction program (http://www.bioinf.manchester.ac.uk/dbbrowser/bioactivity/NPS2.html). Regions predicted to form two helices connected with a loop were selected. This predicted 21 and 17 HEAT repeats in *S. cerevisiae* and human Vac14, respectively. We manually aligned the human Vac14 sequence with random seed sequences from the Pfam database and obtained the same 17 repeats.

Fluorescence microscopy

Yeast cells labelled with FM4-64 (Duex *et al*, 2006a). Fluorescence and differential interference contrast (DIC) images generated with a Deltavision system (Applied Precision, WA). Images are processed using Adobe Photoshop.

Immunoprecipitation in yeast cells

A total of 10 OD log-phase cells were lysed in lysis buffer; 50 mM Tris pH 7.5, 120 mM NaCl, 10 mM EDTA, 1 mM EGTA, 5 mM 2-glycerophosphate, 1 mM PMSF, 10 mM benzamidine, 1 mg/ml leupeptin, 5 mg/ml aprotonin. Extracts were spun at 500 *g* to sediment unbroken cells. Octyl-glucoside (Sigma) was added to the supernatant to a final concentration of 0.5%. Subsequent manipulations were performed at 4 °C. Resulting extracts were incubated for 30 min and spun at 13 000 *g*, 10 min. Anti-HA (COVANCE), anti-GFP (Roche Applied Science) or anti-V5 (Invitrogen) were added to the supernatant and incubated for 1 h. Protein A immobilized on Sepharose beads (Sigma) was added and incubated for 1 h. Protein complexes bound to the beads were washed seven times with lysis buffer containing 0.5% octyl-glucoside, then eluted in sample buffer (50 mM Tris, pH6.8, 2% SDS, 5% β-mercaptoethanol, 10% glycerol, 0.01% BPB) at 80°C, 5 min. SDS–PAGE and western blot analysis were used to detect Vac14–HA or V5, Vac7, Fab1, Fig4–Myc.

Yeast two-hybrid analysis

VAC14 was subcloned into the *Xma*I–*Sal*I site of pGAD or pGBD. *FAB1* encoding amino acids 538–1085 was subcloned into the *Eco*RI–*Bgl*II site of pGBD. *VAC7* encoding amino acids 394–918 was subcloned into *Sma*I–*Sal*I site of pGBD. *ATG18* was subcloned into the *Eco*RI–*Sal*I site of pGBD. *FIG4* was subcloned into the *Bam*HI–*Pst*I site of pGBD. Plasmids were cotransformed into the yeast strain PJ69-4A, transformants were plated onto SC-LEU-TRP, replica-plated onto SC-LEU-TRP, SC-LEU-TRP-ADE-HIS + 3AT, or SC-LEU-TRP-ADE-HIS and grown for 4–10 days at 24°C. The yeast strain PJ69-4A and the pGAD and pGBD vectors have been described (James *et al*, 1996).

Glycerol gradients

A total of 12 ml of 10–50% glycerol gradients were prepared in the lysis buffer with 0.5% octyl-glucoside. S13 lysates were prepared from 20 OD cells as described above, loaded on the top and spun at 31 000 r.p.m. for 18 h at 4°C. Fractions (1 ml) were precipitated with TCA, and 1/10 of the sample was separated by SDS–PAGE.

Supplementary data

Supplementary data are available at *The EMBO Journal* Online (http://www.embojournal.org).

Acknowledgements

We thank Dr Lucia Rameh for the protocol to generate the labelled lipid standards. We thank Drs Yui Jin, Rob Piper, Guy Lenk, Cole Ferguson, and members of the Weisman and Meisler labs for helpful discussions. We thank Emily Kauffman for technical assistance. This work was supported by NIH grants R01-GM50403 to LSW, R01-GM24872 to MHM, T32 GM07544 training grant to CYC, and RRO1183 to the Mouse Mutant Resource at the Jackson Laboratory.

References

Andrade MA, Ponting CP, Gibson TJ, Bork P (2000) Homology-based method for identification of protein repeats using statistical significance estimates. *J Mol Biol* **298:** 521–537

Behnia R, Munro S (2005) Organelle identity and the signposts for membrane traffic. *Nature* **438:** 597–604

Bolis A, Zordan P, Coviello S, Bolino A (2007) Myotubularin-related (MTMR) phospholipid phosphatase proteins in the peripheral nervous system. *Mol Neurobiol* **35:** 308–316

Bonangelino CJ, Catlett NL, Weisman LS (1997) Vac7p, a novel vacuolar protein, is required for normal vacuole inheritance and morphology. *Mol Cell Biol* **17:** 6847–6858

Bonangelino CJ, Nau JJ, Duex JE, Brinkman M, Wurmser AE, Gary JD, Emr SD, Weisman LS (2002) Osmotic stress-induced increase of phosphatidylinositol 3,5-bisphosphate requires Vac14p, an activator of the lipid kinase Fab1p. *J Cell Biol* **156:** 1015–1028

Botelho RJ, Efe JA, Teis D, Emr SD (2008) Assembly of a Fab1 phosphoinositide kinase signaling complex requires the Fig4 phosphoinositide phosphatase. *Mol Biol Cell* **10:** 4273–4286

Bronson R, Perides G, Sweet H, Ward-Bailey PF, Davisson M (2003) Infantile gliosis (ingls) a new spontaneous mutation in the mouse. MGI Direct Data Submission http://mousemutant.jax.org/gliosis_paper.html

Chook YM, Blobel G (1999) Structure of the nuclear transport complex karyopherin-[beta]2-Ran[dot]GppNHp. *Nature* **399:** 230–237

Chow CY, Zhang Y, Dowling JJ, Jin N, Adamska M, Shiga K, Szigeti K, Shy ME, Li J, Zhang X, Lupski JR, Weisman LS, Meisler MH (2007) Mutation of FIG4 causes neurodegeneration in the pale tremor mouse and patients with CMT4J. *Nature* **448:** 68–72

Cingolani G, Petosa C, Weis K, Muller CW (1999) Structure of importin-[beta] bound to the IBB domain of importin-[alpha]. *Nature* **399:** 221–229

Di Paolo G, De Camilli P (2006) Phosphoinositides in cell regulation and membrane dynamics. *Nature* **443:** 651–657

Dove SK, McEwen RK, Mayes A, Hughes DC, Beggs JD, Michell RH (2002) Vac14 controls PtdIns(3,5)P(2) synthesis and Fab1-dependent protein trafficking to the multivesicular body. *Curr Biol* **12:** 885–893

Dove SK, Piper RC, McEwen RK, Yu JW, King MC, Hughes DC, Thuring J, Holmes AB, Cooke FT, Michell RH, Parker PJ, Lemmon MA (2004) Svp1p defines a family of phosphatidylinositol 3,5-bisphosphate effectors. *EMBO J* **23:** 1922–1933

Duex JE, Nau JJ, Kauffman EJ, Weisman LS (2006a) Phosphoinositide 5-phosphatase Fig 4p is required for both acute rise and subsequent fall in stress-induced phosphatidylinositol 3,5-bisphosphate levels. *Eukaryot Cell* **5:** 723–731

Duex JE, Tang F, Weisman LS (2006b) The Vac14p–Fig4p complex acts independently of Vac7p and couples PI3,5P2 synthesis and turnover. *J Cell Biol* **172:** 693–704

Efe JA, Botelho RJ, Emr SD (2007) Atg18 regulates organelle morphology and Fab1 kinase activity independent of its membrane recruitment by phosphatidylinositol 3,5-bisphosphate. *Mol Biol Cell* **11:** 4232–4244

Flanigan K, Gardner K, Alderson K, Galster B, Otterud B, Leppert MF, Kaplan C, Ptacek LJ (1996) Autosomal dominant spinocerebellar ataxia with sensory axonal neuropathy (SCA4): clinical description and genetic localization to chromosome 16q22.1. *Am J Hum Genet* **59:** 392–399

Gary JD, Sato TK, Stefan CJ, Bonangelino CJ, Weisman LS, Emr SD (2002) Regulation of Fab1 phosphatidylinositol 3-phosphate 5-kinase pathway by Vac7 protein and Fig4, a polyphosphoinositide phosphatase family member. *Mol Biol Cell* **13:** 1238–1251

Gary JD, Wurmser AE, Bonangelino CJ, Weisman LS, Emr SD (1998) Fab1p is essential for PtdIns(3)P 5-kinase activity and the maintenance of vacuolar size and membrane homeostasis. *J Cell Biol* **143:** 65–79

Groves MR, Hanlon N, Turowski P, Hemmings BA, Barford D (1999) The structure of the protein phosphatase 2A PR65/A subunit reveals the conformation of its 15 tandemly repeated HEAT motifs. *Cell* **96:** 99–110

Ikonomov OC, Sbrissa D, Shisheva A (2006) Localized PtdIns 3,5-P2 synthesis to regulate early endosome dynamics and fusion. *Am J Physiol Cell Physiol* **291:** C393–C404

James P, Halladay J, Craig EA (1996) Genomic libraries and a host strain designed for highly efficient two-hybrid selection in yeast. *Genetics* **144:** 1425–1436

Liu L, Geisert EE, Frankfurter A, Spano AJ, Jiang CX, Yue J, Dragatsis I, Goldowitz D (2007) A transgenic mouse class-III beta tubulin reporter using yellow fluorescent protein. *Genesis* **45:** 560–569

Matteis MAD, Godi A (2004) PI-loting membrane traffic. *Nat Cell Biol* **6:** 487–492

Perry J, Kleckner N (2003) The ATRs, ATMs, and TORs are giant HEAT repeat proteins. *Cell* **112:** 151–155

Rudge SA, Anderson DM, Emr SD (2004) Vacuole size control: regulation of PtdIns(3,5)P2 levels by the vacuole-associated Vac14-Fig4 complex, a PtdIns(3,5)P2-specific phosphatase. *Mol Biol Cell* **15:** 24–36

Rutherford AC, Traer C, Wassmer T, Pattni K, Bujny MV, Carlton JG, Stenmark H, Cullen PJ (2006) The mammalian phosphatidylinositol 3-phosphate 5-kinase (PIKfyve) regulates endosome-to-TGN retrograde transport. *J Cell Sci* **119:** 3944–3957

Sbrissa D, Ikonomov OC, Fu Z, Ijuin T, Gruenberg J, Takenawa T, Shisheva A (2007) Core protein machinery for mammalian phosphatidylinositol 3,5-bisphosphate synthesis and turnover that regulates the progression of endosomal transport. Novel Sac phosphatase joins the ArPIKfyve-PIKfyve complex. *J Biol Chem* **282:** 23878–23891

Volpicelli-Daley L, De Camilli P (2007) Phosphoinositides' link to neurodegeneration. *Nat Med* **13:** 784–786

Xing Y, Xu Y, Chen Y, Jeffrey PD, Chao Y, Lin Z, Li Z, Strack S, Stock JB, Shi Y (2006) Structure of protein phosphatase 2A core enzyme bound to tumor-inducing toxins. *Cell* **127:** 341–353

Yamamoto A, DeWald DB, Boronenkov IV, Anderson RA, Emr SD, Koshland D (1995) Novel PI(4)P 5-kinase homologue, Fab1p, essential for normal vacuole function and morphology in yeast. *Mol Biol Cell* **6:** 525–539

Zhang X, Chow CY, Sahenk Z, Shy ME, Meisler MH, Li J (2008) Mutation of FIG4 causes a rapidly progressive, asymmetric neuronal degeneration. *Brain* **131:** 1990–2001

Zhang Y, Zolov SN, Chow CY, Slutsky SG, Richardson SC, Piper RC, Yang B, Nau JJ, Westrick RJ, Morrison SJ, Meisler MH, Weisman LS (2007) Loss of Vac14, a regulator of the signaling lipid phosphatidylinositol 3,5-bisphosphate, results in neurodegeneration in mice. *Proc Natl Acad Sci USA* **104:** 17518–17523

